6th European Conference on Computational Mechanics (ECCM 6)
7th European Conference on Computational Fluid Dynamics (ECFD 7)
11-15 June 2018, Glasgow, UK

TIME DISCRETIZATION ERROR ANALYSIS IN MULTIFIELD PLASTICITY

Bettina Schröder[1] **and Detlef Kuhl**[1]

[1] Institute of Mechanics and Dynamics, University of Kassel, Mönchebergstraße 7, 34109 Kassel, schroederbettina@uni-kassel.de, kuhl@uni-kassel.de

Key words: Variational Methods, Multifield Plasticity, Time Discretization Error

Abstract. In the following paper a multifield approach towards elasto(visco)plasticity is derived to enable the application of higher order time integration schemes to the balance of linear momentum and the material laws simultaneously. The numerical implementation of this scheme is based on distinct types of NEWTON procedures as well as on the finite element method. Its functionality is demonstrated by means of a dynamic benchmark example. Therein, two distinct yield limits are assumed to analyze the effect of elasto(visco)plastic switching points. Furthermore, the material models of elastoplasticity and elastoviscoplasticity are opposed. In this context the time discretization error and the orders of convergence of distinct field variables of a third order stiffly accurate diagonally implicit RUNGE-KUTTA method are analyzed.

1 MOTIVATION

In industrial mass production the application of simulation techniques gains increasing importance. On the one hand the evaluation of components concerning their functionality is inevitable, on the other hand the simulation of whole process chains is a crucial topic. An example where both aspects have to be taken into account is the integrated thermomechanical forming process depicted in **Figure 1**. Due to a local inductive heat-

Figure 1: Integrated thermomechanical forming process, cf. [19]

ing, in the first step a non-uniform temperature distribution is achieved. Afterwards the

workpiece is forged and simultaneously cooled due to the contact with the forming die. Within both process steps the evolution of distinct steel phases is enabled, leading to areas with distinct but defined material properties. A further adjustment of the material characteristics is obtained via a partial cooling with a high pressured air stream in the third process step, cf. [19]. Because of the variety of interacting fields and their dynamic behavior high demands on the material modeling as well as on the numerical schemes exist. The first and the last process step are extensively studied in [3, 4] and references therein, while exemplary material models for the second step can be found in [12, 13]. In this paper the focus lies on the numerical realization which is necessary to simulate the second process step. In this context, a variational multifield approach is followed together with a stiffly accurate diagonally implicit RUNGE-KUTTA time integration scheme to dissolve the dynamic behavior. Thereby, the time discretization error as well as the order of convergence of the time discretization scheme are analyzed in dependence of the elasto(visco)plastic switching point and the chosen material formulation. To be able to concentrate on the corresponding effects, simplifications are performed. On the one hand thermal effects are neglected, on the other hand the occurring deformations are limited to the small strain case. Furthermore, the most simple isotropic ideal elastoplastic and elastoviscoplastic material laws presented in [17] are taken into account and the occurring contact with the forming die is disregarded.

2 BASIC EQUATIONS FOR ELASTO(VISCO)PLASTICITY

The mathematical description of an arbitrary continuum mechanical body's deformation is carried out using the balance of linear momentum

$$\rho \ddot{\boldsymbol{u}} = \nabla \cdot \boldsymbol{\sigma} + \rho \boldsymbol{b} \tag{1}$$

together with the NEUMANN and DIRICHLET boundary conditions

$$\boldsymbol{\sigma} \cdot \boldsymbol{n} - \boldsymbol{t}^* = \boldsymbol{0} \qquad\qquad \boldsymbol{u} = \boldsymbol{u}^*. \tag{2}$$

Therein, the volume forces $\rho \boldsymbol{b}$, containing the density ρ, and the divergence of the stress tensor $\boldsymbol{\sigma}$ are linked to the acceleration field $\ddot{\boldsymbol{u}}$. The prescribed stress vector and the displacement vector are denoted by $\boldsymbol{t}^*$ as well as $\boldsymbol{u}^*$, while the outward normal vector of the continuum mechanical body $\mathcal{B}$ is denoted by $\boldsymbol{n}$.
The association of elastoplastic or elastoviscoplastic material behavior to the domain $\mathcal{B}$ is achieved within the context of constitutive laws and evolution equations, [17]. For their formulation an additive decomposition of the linear strain tensor $\boldsymbol{\varepsilon} = \frac{1}{2}\left[\nabla \boldsymbol{u} + \nabla \boldsymbol{u}^{\mathrm{T}}\right]$ into an elastic $\boldsymbol{\varepsilon}_{\mathrm{e}}$ and a (visco)plastic part $\boldsymbol{\varepsilon}_{\mathrm{p}}$

$$\boldsymbol{\varepsilon} = \boldsymbol{\varepsilon}_{\mathrm{e}} + \boldsymbol{\varepsilon}_{\mathrm{p}} \tag{3}$$

is assumed. To distinguish between elastic and (visco)plastic behavior, the VON MISES yield function

$$f = \|\mathrm{dev}\,(\boldsymbol{\sigma})\| - \sqrt{\frac{2}{3}}\sigma_y \tag{4}$$

with the yield stress σ_y is introduced. If the actual stress state yields to values smaller than zero, elastic properties prevail otherwise (visco)plastic properties are predominant. Within the isotropic elastic case the link between stresses and strains is established exploiting the elastic constitutive tensor

$$\mathbb{C} = \lambda \mathbf{1} \otimes \mathbf{1} + 2\mu \mathbb{I}, \tag{5}$$

containing the unity tensors $\mathbf{1} = \delta_{ij} \boldsymbol{e}_i \otimes \boldsymbol{e}_j$ and $\mathbb{I} = \frac{1}{2} \left[\delta_{ik}\delta_{jl} + \delta_{il}\delta_{jk}\right] \boldsymbol{e}_i \otimes \boldsymbol{e}_j \otimes \boldsymbol{e}_k \otimes \boldsymbol{e}_l$ as well as the LAMÉ parameters λ, μ. Hence, the constitutive law

$$\boldsymbol{\sigma} = \mathbb{C} : \boldsymbol{\varepsilon}_{\mathrm{e}} = \mathbb{C} : \left[\boldsymbol{\varepsilon} - \boldsymbol{\varepsilon}_{\mathrm{p}}\right] \tag{6}$$

can be established. The determination of the (visco)plastic strain tensor depends on the type of formulation. In the *plastic* case, the evolution equation and the KUHN-TUCKER conditions with the LAGRANGE multiplier γ

$$\dot{\boldsymbol{\varepsilon}}_{\mathrm{p}} = \gamma \frac{\mathrm{dev}\left(\boldsymbol{\sigma}\right)}{\|\mathrm{dev}\left(\boldsymbol{\sigma}\right)\|} \qquad \text{with} \qquad \gamma \geq 0, f(\boldsymbol{\sigma}) \leq 0, \gamma f(\boldsymbol{\sigma}) = 0 \tag{7}$$

are elaborated. They state, if purely elastic deformations prevail, that $f < 0$ and $\gamma = 0$ have to hold. For *plastic* deformations the examined stress state has to lie on the yield surface with $f = 0$ and $\gamma \geq 0$ has to be fulfilled. Thereby, the LAGRANGE multiplier γ is calculated by solving the consistency condition $\gamma \dot{f} = 0$. The derivation of these assumptions are depicted amongst others in [11, 18].

In the *viscoplastic* case equation (7) is reformulated into

$$\dot{\boldsymbol{\varepsilon}}_{\mathrm{p}} = \gamma \frac{\mathrm{dev}\left(\boldsymbol{\sigma}\right)}{\|\mathrm{dev}\left(\boldsymbol{\sigma}\right)\|} \qquad \text{with} \qquad \gamma = \frac{1}{\chi} \langle f(\boldsymbol{\sigma}) \rangle. \tag{8}$$

Hence, the KUHN-TUCKER conditions are neglected and the LAGRANGE multiplier is prescribed, containing a smoothed version of the yield function

$$\langle f(\boldsymbol{\sigma}) \rangle \coloneqq \begin{cases} f(\boldsymbol{\sigma}) & \text{for} \quad f(\boldsymbol{\sigma}) \geq 0 \\ 0 & \text{for} \quad f(\boldsymbol{\sigma}) < 0. \end{cases} \tag{9}$$

Hence, elastic properties exist if $f < 0$ holds and *viscoplastic* behavior is predominant for $f \geq 0$. Correspondingly, stress states lying outside the yield surface are permitted.

3 MULTIFIELD ACCESS TOWARDS ELASTO(VISCO)PLASTICITY

To determine the behavior of an arbitrary continuum mechanical body possessing elasto(visco)plastic material characteristics as described in the preceding section 2, numerical implementation schemes have to be derived. Herein, a multifield approach is followed which enables the usage of a wide class of higher order accurate time integration schemes for the balance of linear momentum and the material laws, simultaneously, by elevating the latter also on element level. To derive this access, a physically motivated variational principle will be presented and extended to the elasto(visco)plastic regime.

3.1 Principal of Jourdain

Originally, the principal of JOURDAIN was meant to fill the gap between the principle of virtual power and GAUSS' principle of least constraints, cf. [10]. In this paper it will be generalized and extended, assuming that the total power of a system, consisting of the kinetic energy, the internal energy, the power due to external forces and a dissipational potential, reaches a stationary point, cf. [2, 14]. For elastoplasticity this leads to the problem formulation

$$\underset{\dot{\boldsymbol{u}},\dot{\boldsymbol{\varepsilon}}_{\mathrm{p}},\boldsymbol{\sigma},\gamma\geq 0}{\operatorname{stat}} P(\dot{\boldsymbol{u}},\dot{\boldsymbol{\varepsilon}}_{\mathrm{p}},\boldsymbol{\sigma},\gamma). \tag{10}$$

Evaluating the stationarity condition as demonstrated in [22] results in the weak forms

$$\int_{\Omega} \rho_0 \delta\dot{\boldsymbol{u}}\cdot\ddot{\boldsymbol{u}}\,dV + \int_{\Omega} \left[\delta\dot{\boldsymbol{\varepsilon}}\colon \mathbb{C}_{\mathrm{e}}\colon \left[\boldsymbol{\varepsilon}-\boldsymbol{\varepsilon}_{\mathrm{p}}\right]\right] dV - \int_{\Omega} \rho_0 \delta\dot{\boldsymbol{u}}\cdot\boldsymbol{f}\,dV - \int_{\Gamma_{\mathrm{t}^*}} \delta\dot{\boldsymbol{u}}\cdot\boldsymbol{t}^*\,dA = 0, \tag{11}$$

$$\int_{\Omega} \left[\delta\dot{\boldsymbol{\varepsilon}}_{\mathrm{p}}\colon \mathbb{C}_{\mathrm{e}}\colon \left[\boldsymbol{\varepsilon}_{\mathrm{p}}-\boldsymbol{\varepsilon}\right] + \delta\dot{\boldsymbol{\varepsilon}}_{\mathrm{p}}\colon \boldsymbol{\sigma}\right] dV = 0, \tag{12}$$

$$\int_{\Omega} \left[\delta\boldsymbol{\sigma}\colon \dot{\boldsymbol{\varepsilon}}_{\mathrm{p}} - \gamma\delta\boldsymbol{\sigma}\colon \frac{\partial f(\boldsymbol{\sigma})}{\partial\boldsymbol{\sigma}}\right] dV = 0, \tag{13}$$

$$\int_{\Omega} f(\boldsymbol{\sigma})\left[\delta\gamma-\gamma\right] dV \leq 0, \tag{14}$$

with $\delta\gamma \geq 0, \gamma \geq 0$ and $\operatorname{dev}(\boldsymbol{\sigma}) \neq \mathbf{0}$. If $\operatorname{dev}(\boldsymbol{\sigma}) = \mathbf{0}$ holds the LAGRANGE multiplier γ is simply set to zero. Analyzing equations (11)-(14) demonstrates that within this variational multifield approach the balance of linear momentum, the material laws and the yield function are all formulated in a weak sense. Hence, the displacement field, the stresses, the plastic strains and the LAGRANGE multiplier are considered as unknown variables which have to be determined. For elastoviscoplasticity the dissipational potential is slightly modified compared to the elastoplastic case by introducing a penalization term, cf. [14]. Thus, problem (10) is recast into

$$\underset{\dot{\boldsymbol{u}},\dot{\boldsymbol{\varepsilon}}_{\mathrm{p}},\boldsymbol{\sigma}}{\operatorname{stat}} P(\dot{\boldsymbol{u}},\dot{\boldsymbol{\varepsilon}}_{\mathrm{p}},\boldsymbol{\sigma}), \tag{15}$$

yielding

$$\int_{\Omega} \rho_0 \delta\dot{\boldsymbol{u}}\cdot\ddot{\boldsymbol{u}}\,dV + \int_{\Omega} \delta\dot{\boldsymbol{\varepsilon}}\colon \mathbb{C}_{\mathrm{e}}\colon \left[\boldsymbol{\varepsilon}-\boldsymbol{\varepsilon}_{\mathrm{p}}\right] dV - \int_{\Omega} \rho_0\, \delta\dot{\boldsymbol{u}}\cdot\boldsymbol{f}\,dV - \int_{\Gamma_{\mathrm{t}^*}} \delta\dot{\boldsymbol{u}}\cdot\boldsymbol{t}^*\,dA = 0, \tag{16}$$

$$\int_{\Omega} \left[\delta\dot{\boldsymbol{\varepsilon}}_{\mathrm{p}}\colon \mathbb{C}_{\mathrm{e}}\colon \left[\boldsymbol{\varepsilon}_{\mathrm{p}}-\boldsymbol{\varepsilon}\right] + \delta\dot{\boldsymbol{\varepsilon}}_{\mathrm{p}}\colon \boldsymbol{\sigma}\right] dV = 0, \tag{17}$$

$$\int_{\Omega} \left[\delta\boldsymbol{\sigma}\colon \dot{\boldsymbol{\varepsilon}}_{\mathrm{p}} - \delta\boldsymbol{\sigma}\colon \frac{1}{\chi}\left\langle f(\boldsymbol{\sigma})\right\rangle \frac{\partial f(\boldsymbol{\sigma})}{\partial\boldsymbol{\sigma}}\right] dV = 0. \tag{18}$$

Therein, the LAGRANGE multiplier is no primary variable any more and the variational inequality embodied by the yield function is obsolete. Thus, elastoviscoplasticity and elastoplasticity are described by distinct weak forms. But nonetheless within both formulations, the material laws are elevated on structural level and all sorts of equations containing time derivatives can be temporally discretized simultaneously. The price however is, that a large system of equations has to be solved and in the case of elastoplasticity a variational inequality has to be accounted for.

3.2 Spatial discretization

The next step within the variational solution procedure is, the spatial discretization of the weak forms. Therefore, the distinct primary variables are approximated by a number of nodal values and shape functions depending on the natural coordinates. Therefore, two types of approximations are used. While the displacement field is interpolated continuously using LAGRANGE shape functions $N(\boldsymbol{\xi})$, the stress tensor, the plastic strains and the LAGRANGE multiplier are approximated discontinuously using shape functions $\bar{N}(\boldsymbol{\xi})$. Hence, the latter quantities can perform jumps across element boundaries, which is not possible in the continuous case, cf. [16]. Inserting these terms leads to a semidiscrete form, [9, 23].

3.3 Linearization

Due to the behavior of the yield function, a nonlinear system of equations has to be taken into account. Furthermore, in the elastoplastic case even variational inequalities pertain. The solution procedure, therefore, consists of two branches. On all equalities a classical NEWTON-RAPHSON scheme is applied. It is based on a TAYLOR series expansion, which is aborted after the linear term. Thus, the semidiscrete weak form is linearized, exploiting the GÂTEAUX derivative, cf. [8, 21]. For the inequalities a semi-smooth NEWTON process is carried out. Therein, the included inequality is first transformed into an equality by means of a nonlinear complementarity function, afterwards, a special kind of linearization is performed, introducing an active set strategy. The result is the following system of equations on structural level

$$\bar{\mathbf{M}}\Delta\ddot{\mathbf{w}} + \bar{\mathbf{D}}\Delta\dot{\mathbf{w}} + \bar{\mathbf{K}}\Delta\mathbf{w} = \bar{\mathbf{R}}^* - \bar{\mathbf{R}}, \tag{19}$$

$$\gamma^{i,k+1} = 0 \qquad \forall i \in \mathcal{I}^k, \tag{20}$$

$$\mathcal{A}^{k+1} := \{i | \gamma^{ei,k+1} + c\, \bar{r}_\gamma^{ei,k+1} > 0\}, \tag{21}$$

$$\mathcal{I}^{k+1} := \{i | \gamma^{ei,k+1} + c\, \bar{r}_\gamma^{ei,k+1} \leq 0\}. \tag{22}$$

with the suitable tangent matrices $\bar{\mathbf{M}}, \bar{\mathbf{D}}, \bar{\mathbf{K}}$, load vectors $\bar{\mathbf{R}}, \bar{\mathbf{R}}^*$ and active as well as inactive sets $\mathcal{A}, \mathcal{I}$, cf. [15]. The variable $\mathbf{w}$ represents the vector of primary variables, consisting of the displacements, the plastic strains, the stresses and the LAGRANGE multiplier.

Within the elastoviscoplastic formulation only variational equalities prevail, hence, in that case the application of a classical NEWTON-RAPHSON scheme is sufficient and results in a similar weak form as depicted in equation (19), but equations (20)-(22) are obsolete.

3.4 Time discretization

Before the systems of equations (19) as well as (20)-(22) can be solved, a temporal discretization has to be carried out. In this paper this is done considering stiffly accurate diagonal implicit RUNGE-KUTTA schemes. The idea behind this class of methods is to divide the time period of interest $[t_0, T]$ into time intervals $[t_n, t_{n+1}]$ with the time step size Δt. Moreover, each time step contains s stages at $t_{ni} = t_n + c_i \Delta t$ for $i = 1, ..., s$, whereby the last stage is identical to the end of the time step $t_{ns} = t_{n+1}$. The parameters c_i are RUNGE-KUTTA coefficients. Besides it is assumed, that at all stages equation (19) as well as (20)-(22) have to hold. The stage variables are then approximated using special quadrature rules and weighting factors a_{ij}, cf. [5, 6].

$$\dot{\boldsymbol{w}}_{ni} = \dot{\boldsymbol{w}}_n + \Delta t \sum_{j=1}^{i-1} a_{ij} \ddot{\boldsymbol{w}}_{nj} + \Delta t a_{ii} \ddot{\boldsymbol{w}}_{ni} = \dot{\boldsymbol{W}} + \Delta t a_{ii} \ddot{\boldsymbol{w}}_{ni} \tag{23}$$

$$\boldsymbol{w}_{ni} = \boldsymbol{w}_n + \Delta t \sum_{j=1}^{i-1} a_{ij} \dot{\boldsymbol{w}}_{nj} + \Delta t a_{ii} \dot{\boldsymbol{w}}_{ni} = \boldsymbol{W} + \Delta t a_{ii} \dot{\boldsymbol{w}}_{ni} \tag{24}$$

For the stage increments equations (23)-(24) are adapted, too. The result is the fully discretized and linearized form

$$\left[\frac{1}{[a_{ii} \Delta t]^2} \bar{\mathbf{M}}_{ni} + \frac{1}{[a_{ii} \Delta t]} \bar{\mathbf{D}}_{ni} + \bar{\mathbf{K}}_{ni} \right] \Delta \mathbf{w}_{ni} = \bar{\mathbf{R}}^*_{ni} - \bar{\mathbf{R}}_{ni}, \tag{25}$$

$$\gamma^{i,k+1}_{ni} = 0 \qquad \forall i \in \mathcal{I}^k, \tag{26}$$

$$\mathcal{A}^{k+1} := \{ i | \gamma^{ei,k+1}_{ni} + c\, \bar{r}^{ei,k+1}_{\gamma,ni} > 0 \}, \tag{27}$$

$$\mathcal{I}^{k+1} := \{ i | \gamma^{ei,k+1}_{ni} + c\, \bar{r}^{ei,k+1}_{\gamma,ni} \leq 0 \}, \tag{28}$$

so that in each iteration the primary variable vector $\mathbf{w}$ and its time derivatives can be determined. In the elastoplastic case, the active and inactive sets are updated additionally. For elastoviscoplasticity equations (26)-(28) are neglected.

4 DYNAMIC BENCHMARK EXAMPLE

In order to show the functionality of the multifield approach and to evaluate the behavior of the time discretization scheme a small dynamic example is calculated. It is motivated by the integrated thermomechanical forming process depicted in **Figure 1**. Due to the shaft's rotational symmetry a polar coordinate system with the basis vector $\boldsymbol{g}_R$ in radial, $\boldsymbol{g}_Z$ in axial and $\boldsymbol{g}_\Phi$ in tangential direction is introduced, see **Figure 2**. Additionally, a

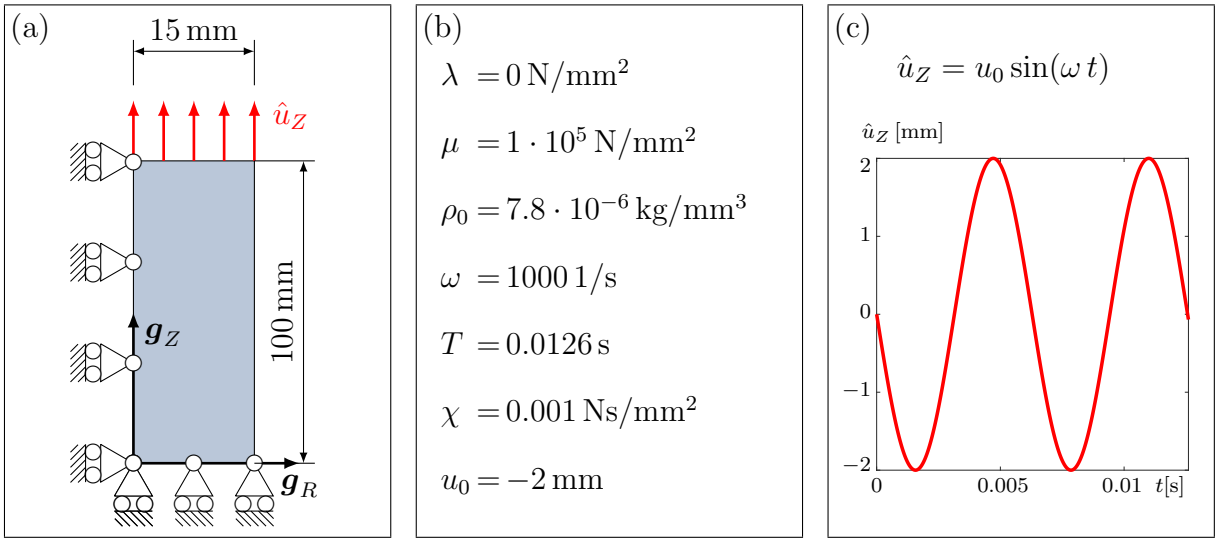

Figure 2: (a) Sketch of the steel shaft and its dimensioning (b) Simulation parameter, (c) Prescribed displacement $\hat{u}_Z$

displacement based load $\hat{u}_Z$ pointing in the shaft's longitudinal direction $\boldsymbol{g}_Z$ is assumed. Hence, an arbitrary meridian half plane with $\Phi = const.$ can be taken into account to describe the steel shaft's properties and the displacement field is solely characterized by its radial and axial components $\boldsymbol{u}(\boldsymbol{X}) = [u_R, u_Z]$. Further necessary model and simulation parameters are also depicted in **Figure 2**. The spatial discretization is based on two finite elements in $\boldsymbol{g}_Z$- and one finite element in $\boldsymbol{g}_R$-direction. For time discretization a third order accurate diagonally implicit RUNGE-KUTTA method (DIRK (3)) is applied, cf. [6]. In order to characterize the behavior of the time integration scheme, two cases are studied for the elastoplastic and the elastoviscoplastic material model. On the one hand a yield stress of $\sigma_y = 900\mathrm{N/mm^2}$ is chosen to represent steel, on the other hand a yield stress of $\sigma_y = 0.01\mathrm{N/mm^2}$ is considered, leading to an instantaneous yielding. Using this election the influence of the elasto(visco)plastic switching point can be depicted and the effect of the viscous regularization can be demonstrated, if the time discretization error and the order of convergence are examined.

5 TIME DISCRETIZATION ERROR ANALYSIS

The quality of a considered time integration scheme is determined by its error behavior and its order of convergence. Since in general no analytical solutions are available, the former has to be estimated. Therefore, a variety of methods exists. In this paper the local and the global h-error

$$\mathbf{e}_{\mathrm{h},n+1} \approx \mathbf{w}_{n+1}^{\Delta t/2}(\mathbf{w}_n) - \mathbf{w}_{n+1}(\mathbf{w}_n) \qquad \mathbf{e}_{\mathrm{h},n+1}^{\mathrm{glob}} \approx \mathbf{w}_{n+1}^{\Delta t/16}(\mathbf{w}_0) - \mathbf{w}_{n+1}(\mathbf{w}_0) \tag{29}$$

are evaluated. Their definition is based on the idea, that with decreasing time step size the error decreases. The estimation is thus founded on numerical comparative solutions $\mathbf{w}_{n+1}^{\Delta t/n}$ computed by using the time step size Δt reduced by a factor two and a factor 16, cf. [3]. A further difference between both error definitions in (29) is, that for the global

h-error only the initial condition is passed, while for the local h-error the results of various intermediate time steps are transferred characterizing the error only within one single time step. Additionally, error characterizing quantities are established to enable the evaluation of the time integration error and the order of convergence for a given problem. In order to be able to make a statement regarding the total time discretization error of distinct unknowns, the norm of the respective error vector is evaluated for various time step sizes at common points in time. Correspondingly, the following quantity is established

$$e_{\mathrm{h},n+1} = \|\mathbf{e}_{\mathrm{h},n+1}\| \,. \tag{30}$$

To estimate the order of convergence numerically, a measure has to be defined to characterize the temporal evolution of the error estimates in (30), so that a relation to a fixed time step size can be established. For this purpose

$$q_{\mathrm{h}} \quad = \mathrm{mean}\left(\text{linear fit}\left(\log(\Delta t), \log\left(e_{\mathrm{h},n+1}(\Delta t)\right)\right)\right). \tag{31}$$

is considered. The idea behind the approach is to calculate the respective error estimator for a variety of time step sizes, install a link between the latter and the error characterizing value in (30), identify the resulting slope by a linear regression in the logarithmic space and determine the order of convergence by averaging, cf. [1]. This procedure is applied to the error estimates obtained by calculating the dynamic examples introduced in section 4. In **Figure 3** the error curves for the displacement field, the stresses and the plastic strains are depicted for four distinct time step sizes. Thereby, **Figure 3** (a)-(c) represent the results for the elastoviscoplastic material formulation using the multifield approach (multi visco) assuming a yield stress of $\sigma_y = 900\mathrm{N/mm^2}$. **Figure 3** (d)-(f) demonstrates the corresponding results for the elastoplastic approach (multi). The error curves for the elastoviscoplastic (multi visco) and the elastoplastic model (multi) with yield stress $\sigma_y = 0.01\mathrm{N/mm^2}$ are shown in **Figure 3** (g)-(i) and **Figure 3** (k)-(m), respectively. All results have in common, that with decreasing time step size the error gets smaller. Furthermore, the average error of the stress field is higher than the one of the plastic strains and of the displacement field. Comparing the elastoviscoplastic to the elastoplastic curves, illustrates only small differences for the displacement field while bigger discrepancies are perceptible for the other two variables. Additionally, if the corresponding plots with distinct yield stresses are opposed, it can be seen that the curves for $\sigma_y = 0.01\mathrm{N/mm^2}$ are much smoother than those obtained with $\sigma_y = 900\mathrm{N/mm^2}$. However, for small time step sizes the former show oscillations, which may be attributed to the numerically challenging yield stress close to zero. The orders of convergence associated to the plots in **Figure 3** are summarized in Table 1. While the order of convergence for the elastoplastic model (multi) determined by the local error estimator lies around the theoretically possible order of three for all analyzed field variables, in the elastoviscoplastic case (multi visco) the plastic strains and the stresses suffer from an order reduction. This behavior is also observed for the orders of convergence if a yield stress of $\sigma_y = 0.01\mathrm{N/mm^2}$ is taken into account. However, if the global error estimator is exploited to calculate the order of convergence distinct results are obtained. For the elastoplastic (multi) and the elastoviscoplastic model

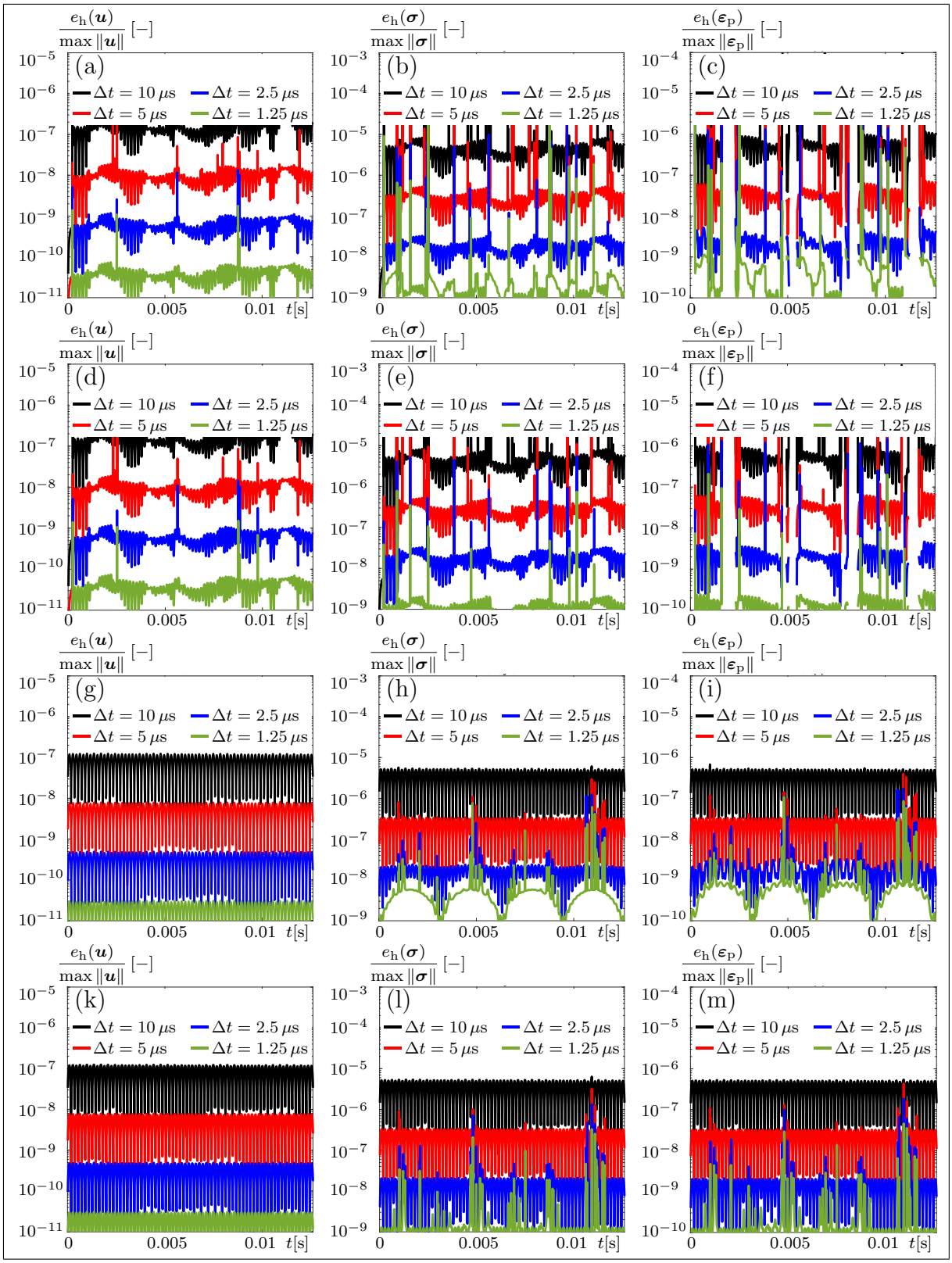

Figure 3: Local time discretization error of the h-method for the displacement, the (visco)plastic strain and the stress field: (a)-(c) DIRK(3) multi visco, DIRK(3) multi, (g)-(i) DIRK(3) multi visco $\sigma_y = 0.01\text{N/mm}^2$, (k)-(m) DIRK(3) multi $\sigma_y = 0.01\text{N/mm}^2$

(multi visco) with a yield stress of $\sigma_y = 900\text{N/mm}^2$ all field variables suffer from an order reduction, while the models with a yield stress of $\sigma_y = 0.01\text{N/mm}^2$ pertain their theoretical order of three. From these observations two conclusions can be drawn. The viscous regularization seems to have no positive effect on the time discretization error. Moreover, the existence of an elasto(visco)plastic switching point influences the order of convergence. The positive impact on the globally determined order of convergence was already shown in [1]. The deterioration of the locally estimated order of convergence seems to be linked to the numerical difficulties associated to the yield stress being close to zero, since the oscillations occur at small time step sizes. Apart from the multifield approach also the conventional access towards elastoplasticity (con) and elastoviscoplasticity (con visco) following the implementation in [17] is simulated. Therein, almost identical results are obtained. The corresponding orders of convergence are depicted in Table 1, too. Hence, the order reduction is not associated to the multifield approach, although it does also not cure it.

Table 1: Estimation of the order of convergence of various time integrators for distinct fields and different error measurements within elasto(visco)plasticity

	$q_{\text{h}}(\mathbf{u})$	$q_{\text{h}}(\boldsymbol{\varepsilon}_{\text{p}})$	$q_{\text{h}}(\boldsymbol{\sigma})$	$q_{\text{h}}^{\text{glob}}(\mathbf{u})$	$q_{\text{h}}^{\text{glob}}(\boldsymbol{\varepsilon}_{\text{p}})$	$q_{\text{h}}^{\text{glob}}(\boldsymbol{\sigma})$
DIRK(3) con	2.99	2.94	2.99	2.26	2.21	2.53
DIRK(3) multi	2.99	2.94	2.99	2.26	2.17	2.53
DIRK(3) con $\sigma_y = 0.01\text{N/mm}^2$	2.99	2.44	2.53	3.06	3.06	3.06
DIRK(3) multi $\sigma_y = 0.01\text{N/mm}^2$	2.99	2.50	2.58	3.06	3.06	3.06
DIRK(3) con visco	2.99	2.17	2.51	2.28	2.23	2.55
DIRK(3) multi visco	3.00	2.18	2.52	2.38	2.32	2.53
DIRK(3) con visco $\sigma_y = 0.01\text{N/mm}^2$	2.99	2.54	2.68	3.06	3.06	3.06
DIRK(3) multi visco $\sigma_y = 0.01\text{N/mm}^2$	2.99	2.55	2.69	3.06	3.06	3.06

6 CONCLUSION AND OUTLOOK

In this paper a variational multifield approach towards elasto(visco)plasticity and its numerical implementation involving stiffly accurate diagonally implicit Runge-Kutta schemes is presented. It is based on extending the principle of virtual power to dissipative systems and thus arranging that the material laws and the balance of linear momentum are on the same solution level. The motivation thereby is founded on the necessity to use higher order time integration schemes in the context of elasto(visco)plasticity, which is drastically simplified with this multifield approach. To demonstrate its functionality distinct dynamic examples are simulated. Additionally, the time discretization error of a specific third order Runge-Kutta scheme is analyzed to compare different estimation

techniques and to show the influence of the elasto(visco)plastic switching point. The order of convergence obtained by the local error is significantly influenced by the choice of yield stress and the material properties. For the elastoplastic case a yield stress reduction leads to a reduction of the order of convergence for the stress and the plastic strain field. In the elastoviscoplastic case a completely contrary behavior is observed. For the displacement field identical orders are obtained for all cases. The globally estimated orders of convergence of the elastoplastic case are similar to those of the elastoviscoplastic case. Evaluating the examples where no elasto(visco)plastic switching point exists, demonstrates that for the global error theoretical orders of convergence of three are obtained. Hence, the observations of [1] can be testified. Thus, the creation and implementation of an appropriate switching point detection strategy is necessary to obtain higher orders of convergence in elasto(visco)plasticity. Therefore, also the usage of adaptive schemes should be investigated. Another open question is, why the viscous regularization did not improve the order of convergence. A similar behavior was already demonstrated in [7]. Additionally, the discrepancies between local and global error estimators have to be examined. In general their behavior should be similar, following [20], which is, within this examples, not the case.

REFERENCES

[1] Eidel, B. and Kuhn, C. Is there an order-barrier $p \leq 2$ for time integration in computational elasto-plasticity? (2015)

[2] Germain, P. The method of virtual power in continuum mechanics. Part 2: Microstructure. *SIAM Journal on Applied Mathematics* (1973) **25**, pp. 556-576.

[3] Gleim, T. *Simulation of Manufacturing Sequences of Functionally Graded Structures.* kassel university press, (2017)

[4] Gleim, T. and Kuhl, D. Electromagnetic Analysis Using Higher Order Numerical Schemes in Space and Time. *Archives of Computational Methods in Engineering* (2018) https://doi.org/10.1007/s11831-017-9249-9.

[5] Hairer, E., S.P. Nørsett and Wanner, G. *Solving Ordinary Differential Equations I. Nonstiff Problems.* Springer-Verlag, (2008).

[6] Ellsiepen, P. and Hartmann, S. Remarks on the interpretation of current non-linear finite element analyses as differential-algebraic equations. *International Journal for Numerical Methods in Engineering* (2001) **51**, pp. 679–707.

[7] Hartmann, S. and Bier, W. High-order time integration applied to metal powder plasticity. *International Journal of Plasticity* (2007) **24**, pp. 17–54.

[8] Holzapfel, G. A. *Nonliner Solid Mechanics.* John Wiley & Sons, (2000).

[9] Hughes, T. J. R *The Finite Element Method. Linear Static and Dynamic Finite Element Analysis.* Dover Publications, INC, (2000).

[10] Jourdain, P. E. B. Note on an Analogue of Gauß' Principle of Least Constraints. *Archive of Applied Mechanics* (1909) **40**, pp. 153-157.

[11] Luenberger, D. G. *Introduction to linear and nonlinear programming*. Addison-Wesley, (1973).

[12] Mahnken, R. and Schneidt, A. A thermodynamic framework and numerical aspects for transformation-induced plasticity at large strains. *Archive of Applied Mechanics* (2009) **80**, pp. 229–253.

[13] Mahnken, R. and Schneidt, A. and Tschumak, S. and Maier, H.J. On the simulation of austenite to bainite phase transformation. *Computational Material Science* (2011) **50**, pp. 1823–1829.

[14] Miehe, C. Mixed variational principles for the evolution problem of gradient-extended dissipative solids. *GAMM-Mitteilungen* (2012) **35**, pp. 8-25.

[15] Popp, A., Gee, M. W. and Wall, W. A. A finite deformation mortar contact formulation using primal-dual active set strategy. *International Journal of Numerical Methods in Engineering* (2009) **79**, pp. 1354-1391.

[16] Schrder, B. and Kuhl, D. Small strain plasticity: classical versus multifield formulation. *Archive of Applied Mechanics* (2015) **85**, pp. 11271145.

[17] Simo, J. C. and Hughes, T. J. R. *Computational Inelasticity*. Springer Verlag, (1997).

[18] Simo, J. C. *Numerical Analysis and Simulation of Plasticity*. Elsevier, (1998).

[19] Steinhoff, K, Weidig, U. and Saba, N., *Investigation of Plastic Forming Under the Influence of Locally and Temporally Variable Temperature and Stress States* in Functionally Graded Materials in Industrial Mass Production. Verlag Wissenschaftliche Scripten, (2009)

[20] Strehmel, K., Weiner, R. and Podhaisky, H. *Numerik gewöhnlicher Differentialgleichungen*. Springer Spektrum, (2012).

[21] Wriggers, P. *Nonlinear Finite Element Methods*. Springer-Verlag, (2008).

[22] Zeidler, E. *Nonlinear Functional Analysis and its Applications III*. Springer Verlag, (1985).

[23] Zienkiewicz, O.C. and Taylor, R.L. *The finite element method*. McGraw Hill, Vol. I., (1989), Vol. II., (1991).